PROCEEDINGS, 51st Workshop on Geothermal Reservoir Engineering
Stanford University, Stanford, California, February 9-11, 2026
SGP-TR-230

Experimental Evaluation of Thermal Cycling Effects on Class G Cement Interfacial Bonding for Geothermal Well Integrity

[1]Andres Felipe Baena Velásquez, [1]Khizar Abid, Diego de la Cruz, Catalin Teodoriu

[1]Mewbourne School of Petroleum and Geological Engineering, The University of Oklahoma, Norman, OK, USA

cteodoriu@ou.edu

Keywords: Geothermal, Interfacial Debonding, Wetting phase, Well Integrity, Temperature Cycles

ABSTRACT

As the world population increases by the day, so does the energy demand. Along with this phenomenon, global warming is taking its toll on the climate. Therefore, to address these issues, sustainable and green energy production is required, in which geothermal energy plays a crucial role. It is a clean, renewable, and continuous source of energy that remains in operation mode for more than 90% of the time and is not weather-dependent. To ensure the smooth transition of energy from the subsurface to the well head, the well integrity has to be assured. The main component that controls well integrity is the well cement and casing. In a geothermal environment, these barriers are exposed to severe thermal cycling and high-temperature gradients that can induce mechanical stress, create microannuli, and impact long-term material degradation, posing significant risks to well integrity. Therefore, it is important to properly analyze cement properties before placing it in the geothermal well. In that respect, this paper presents the experimental results of the impact of thermal loading on the interfacial bonding strength of the Class G cement, which is the most commonly used cement in the wells. The method utilizes a novel apparatus that incorporates an ISCO pump to quantify the interfacial debonding strength of the cement. The preparation of the cement was according to the API standard, after which it was poured into 2-inch diameter, 6-inch long steel pipes and was cured for 14 days. To simulate the geothermal well condition, the samples were exposed to 5 and 10 thermal cycles loading at 95 °C. In one cycle, there is 1 hour of heating and 3 hours of cooling. From the testing, it was noted that before the debonding of the sample occurs, a leakage of water, termed the "wetting phase," is observed at a pressure lower than that of the interfacial debonding pressure. It was also observed that cyclic loading had an impact on the debonding strength, which decreased as the number of cycles increased. Hence, it was concluded that the primary mode of failure was caused by shear debonding, which is facilitated by the creation of microannuli at the interface between the casing and the cement, and is exacerbated by thermal loading. Therefore, before cement placement, it should be ensured that the cement debonding strength is sufficient to resist thermal loading and maintain its integrity throughout the project's life. Otherwise, the subsurface fluid can make its way to shallower formations and ultimately reach the surface, which will jeopardize the success of the geothermal project.

1. INTRODUCTION

To ensure safe and sustainable operations in geothermal and oil and gas wells, it is necessary to focus efforts on maintaining well integrity. In this context, cement plays an important role as a primary barrier to prevent fluid migration, ensure zonal isolation, and maintain the mechanical stability of the well throughout its cycle life (Phi et al., 2019). However, the inherent operating conditions of geothermal systems such as high temperatures, repetitive thermal cycles, high thermal gradients, and the presence of hot fluids (Sprung, 2000; Arbad et al., 2022) represent a significant challenge to the long-term performance of cement during the production, plug, and abandonment phases.

Several studies have demonstrated that exposure to thermal gradients can induce significant stresses at the cement–casing interface due to differences in the thermal expansion coefficients of these materials (Lambrescu et al., 2024; Patel et al., 2025; Albawi et al., 2014; Arbad et al., 2022). This phenomenon can lead to the formation of microcracks, loss of interfacial bonding, and microannulus development, thereby compromising the sealing capacity of the system and increasing the risk of fluid migration. Previous investigations have documented that the progressive deterioration of cement under thermal conditions can result in a significant reduction in its mechanical strength and its ability to maintain the structural integrity of the well. For instance, Vrålstad et al., 2015 conducted a study on 35% (By Weight of Cement) silica flour + Class G cement composite placed between casing and sandstone and shale formations. The analysis revealed a progressive increase in cracks that eventually interconnected to form leakage pathways, which were quantified using 3D CT imaging, thereby compromising zonal isolation. De Andrade et al., 2015 concluded that cement degradation is dominated by cracking caused by shear–compression mechanisms. Using a pressurized cell combined with CT imaging for 10 thermal cycles between 41 and 110 °C, it was found that thermal cycling enlarges pre-existing defects and reduces bonding strength, particularly in sandstone formations. Furthermore, Arbad et al., 2022 confirmed in a review of geothermal studies that Portland Class G cement is prone to strength loss, microcracking, and material alteration at temperatures above 350 °C, leading to increased debonding and fluid migration under real operational conditions.

Despite the advances reported in the literature, a large portion of existing studies has focused on static evaluations or simulations of cement bonding using push-out or direct tensile tests without repetitive thermal cycling (Lambrescu et al., 2024; Kurdowski, 2014), or on short-term experiments limited to 10–20 thermal cycles without progressive monitoring of interfacial debonding (De Andrade et al., 2015; Vrålstad et al., 2015; Fischer & Moghadam, 2023).

In this context, the present article experimentally investigates the effect of thermal cycling on the interfacial bonding strength of Class G cement used in geothermal and oil and gas well cementing operations. Three scenarios were evaluated using 0, 5, and 10 thermal cycles

at 95 °C. Each thermal cycle was defined as one hour of heating followed by three hours of cooling. Subsequently, an ISCO pump was used to apply pressure from the bottom of the specimen in order to quantify the wetting pressure (which is defined as the pressure at which the surface of the sample gets wet due to the water leakage through the defect in the cement matrix or through the interface channel between the casing and cement) and the cement debonding pressure. The results showed that thermal cycles affect the bond between cement and casing, reducing interfacial bonding by up to 34%. This study will help to achieve a better understanding of cement behavior under conditions of geothermal applications

2. MATERIAL AND METHODS

2.1 MATERIAL USED

For the purposes of this experiment, a neat Class G cement was used, following all procedures established by the (API, 2005). The mixed cement was poured into cylindrical molds assembled on a threaded flange, and each sample was subsequently placed in a water bath for curing. To simulate geothermal well conditions, each mold was exposed to heating cycles for one hour followed by cooling cycles for three hours.

The specimens were heated using two thermal jackets attached to the pipe, which were separated by an aluminum ring with the objective of dissipating heat through both the pipe and the cement. The thermal jackets were connected to a CHISHUN NHT-4000W AC voltage regulator (0–220 V), which in turn was connected to a WILLHI digital temperature controller (plug-in thermostat) that was connected to a digital timer responsible for controlling the cycle durations. Figure 1 shows two specimens exposed to thermal cycles.

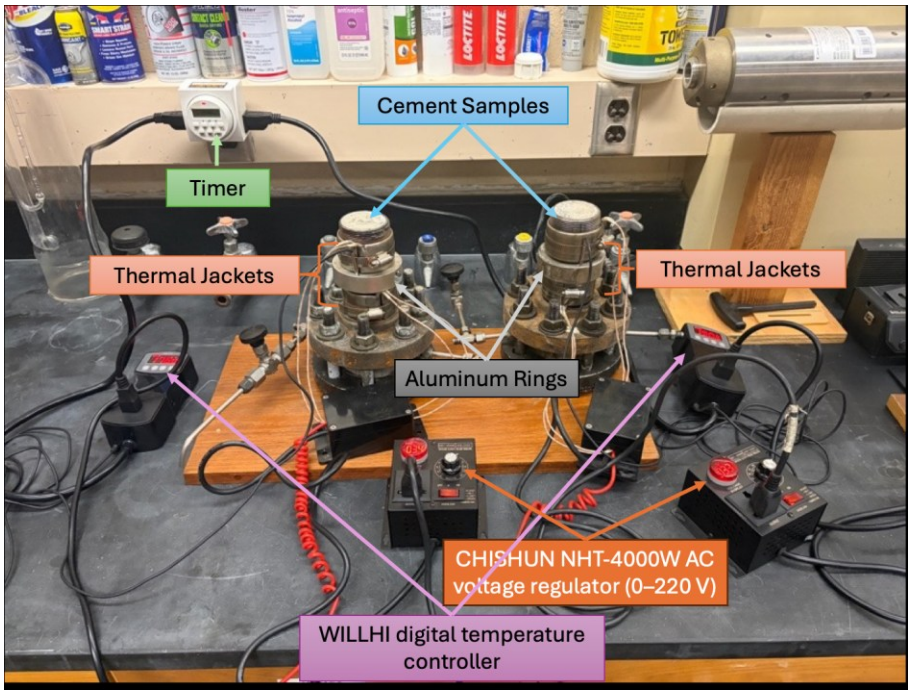

Figure 1 Class G cement samples under thermo-cycles.

Subsequently, the pipe assembled to the threaded flange was seated on an aluminum spacer with two lateral ¼-inch outlets equipped with a drain valve that allowed the passage of the testing fluid (water) for this experiment. Figure 2 displays how the spacer was positioned on top of a blind flange. The flanges were joined using eight bolts, which were torqued to 120 lb-in. Through the pipes and fittings, the samples were connected to the testing setup, which consisted of an ISCO pump Syrinx controller that supplied the testing fluid at a constant flow rate during the test, and a digital pressure sensor that recorded pressure readings.

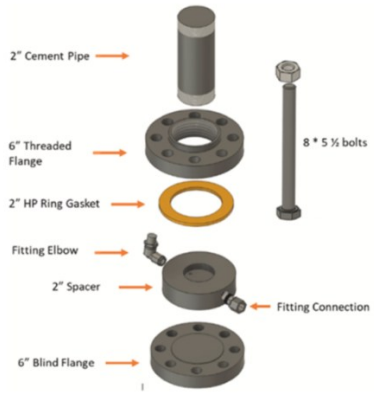

Figure 2 Pipe assembly schematic. (Abid et al., 2025

A digital displacement sensor was placed at the top of the cement sample to record cement core displacement when debonding occurred. For data recording, both sensors were connected to a DAQ system and configured using DASYLab software to log pressure and displacement data throughout the test.

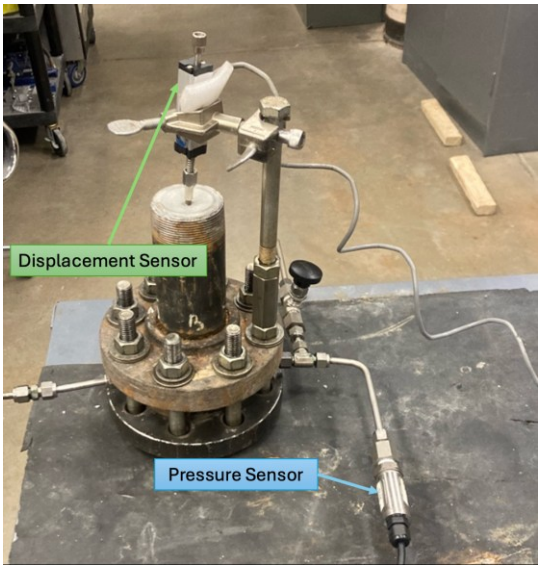

Figure 3 Displacement and pressure sensors on a cement sample.

2.2 Sample Preparation and Curing Procedure

As mentioned in the previous subsection, the samples were mixed following the (API, 2005). For each cement sample, 792.72 grams of Class G cement and 348.53 grams of distilled water were mixed for 50 seconds. During the first 15 seconds, the cement was mixed at 4,000 RPM, and during the remaining 35 seconds, it was mixed at 12,000 RPM. After mixing, the slurry was poured into cylindrical steel molds with a diameter of 2 inches and a length of 6 inches. The samples were placed in a water bath at ambient temperature for 14 days.

After completing the curing period in water, the samples were removed from the water bath and prepared for thermal cycling. Depending on the number of cycles, the samples were exposed to one or two days of curing under dry conditions.

2.3 Thermal Cycling Procedure

Two different thermal cycling conditions (5 and 10 cycles) were evaluated in this experiment. In addition, samples that were not exposed to any temperature variation were also analyzed and served as control samples. For any of the thermal cycle tests, the specimen was connected to the thermal cycling setup through the thermal jackets.

The timer was then programmed according to the number of cycles to which the sample was exposed. The temperature started at room conditions, and the target temperature was 95 °C. The time required to reach the target temperature averaged 23 minutes, as reported in our previous study (Abid et al., 2025).

After completing one full thermal cycle, the procedure was repeated until the required number of cycles for the test was reached. Approximately 24 continuous hours were required for the 5-cycle test and nearly 48 hours for the 10-cycle test.

2.4 Testing Procedure

Once the samples had completed the curing period and undergone the specified number of thermal cycles, the specimen was connected to the testing setup via one of the lateral outlets on the spacer. The displacement sensor was then installed at the top of the sample, as previously described.

To ensure that the system did not contain air that could generate erratic readings, the system was flushed from the ISCO pump (Figure 4) to the drain valve by pumping approximately 100 mL of water. When a constant water flow was observed, the pump was stopped and the drain valve was closed.

With the system fully filled with the testing fluid, DASYLab was activated and the flow rate was set to 2 mL/min. The recording in DASYLab began immediately upon activation of the ISCO pump. The wetting pressure was then visually identified, and the test continued until cement displacement was detected, at which point the test was terminated.

.

Figure 4 Isco pump used in the testing setup.

2.5 Experimental Setup Description.

For this experiment, the experimental setup consisted of two separate components: the thermal cycling setup and the testing setup. Figure 5 presents a schematic diagram of the thermal cycling setup. The sample is connected through two thermal jackets separated by an aluminum ring. The thermal jackets are connected to a voltage regulator, which controls the heating intensity. This regulator is connected to the temperature controller, which limits the temperature between a minimum of 90 °C and a maximum of 95 °C. Finally, the controller is connected to a timer, which is connected to the power source and is responsible for controlling the duration of each cycle.

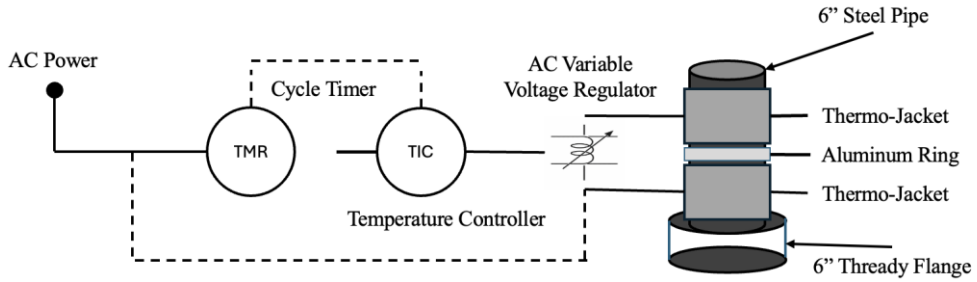

Figure 5 Schematic of thermo-cycling setup.

Figure 6 shows the schematic of the testing setup. The ISCO pump is connected through one of the lateral outlets of the spacer. On the second lateral outlet, a T-connection links the drain valve and the pressure sensor, which is connected to the DAQ system. The DAQ system also receives the signal from the displacement sensor positioned on top of the cement sample. The DAQ terminal is connected to the computer.

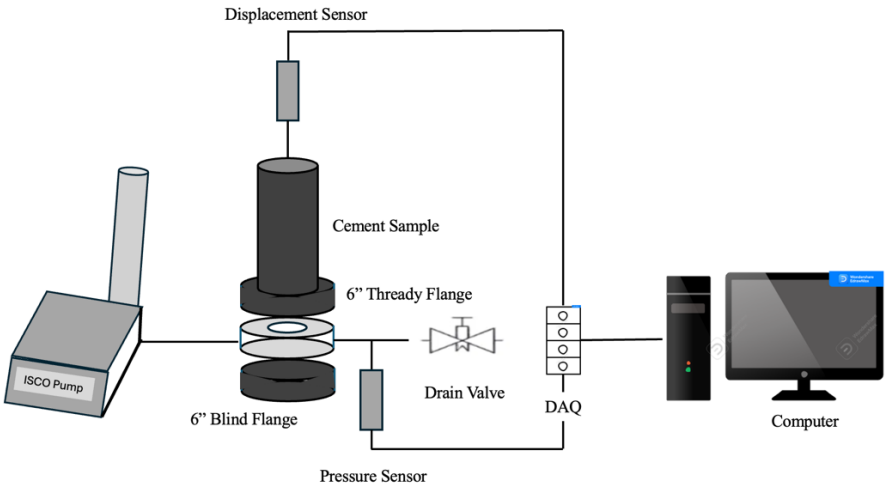

Figure 6: Schematic testing setup.

The final workflow for both control samples and thermal-cycling samples can be observed in the following figure.

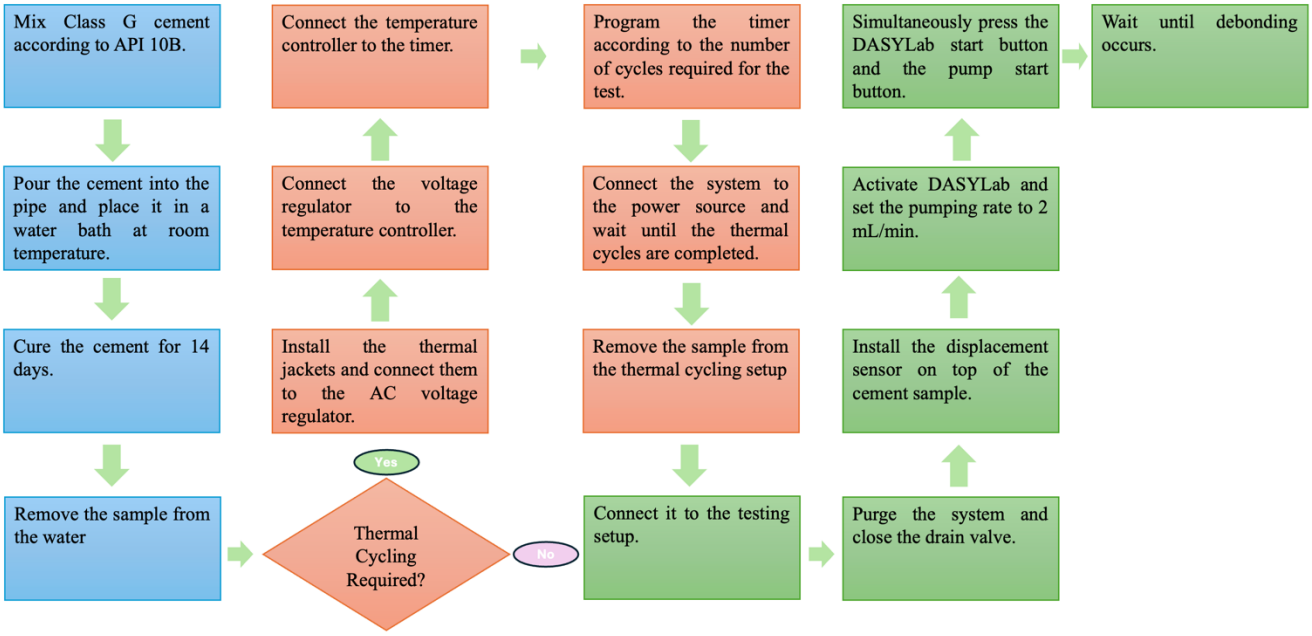

Figure 7: Testing Experimental workflow.

3. RESULTS

As discussed throughout this study, three scenarios were evaluated in this experimental program. The first scenario corresponds to the control tests, which represent the baseline conditions for each specimen under wet and dry curing. This distinction was necessary because specimens exposed to thermal cycling may remain under dry curing conditions for either one or two days, depending on the number of thermal cycles applied. The second scenario includes specimens subjected to five thermal cycles, as described previously. Finally, the third scenario corresponds to specimens exposed to ten thermal cycles. The results for each of these scenarios are presented below.

3.1 Control Samples

Figure 8 presents the average results for specimens cured for 14 days in a water bath, followed by additional curing under dry conditions. The first subgroup corresponds to specimens that were not exposed to dry curing conditions. The second subgroup includes specimens subjected to one additional day of dry curing, and the third subgroup represents specimens subjected to two additional days of dry curing. The blue bars represent the specimens' wetting pressure, while the orange bars represent their debonding pressure. Table 1 lists the control samples to be compared with the thermal-cycle samples.

Table 1: Control sample to be compared with thermal cycle samples

Wet Curing (Days)	Dry Curing (Days)	Compared with the thermal cycle sample
14	-	5 and 10
14	1	5
14	2	10

It can be observed that specimens not exposed to dry conditions exhibit higher bonding strength than those exposed to a dry environment, and that the wetting pressure decreases as the number of days exposed to dry conditions increases. These results indicate that the highest debonding pressure is observed in specimens not subjected to dry conditions (1191 psi), followed by specimens exposed to one day of dry curing (1104 psi), and finally by specimens exposed to two days of dry conditions (978 psi). Additionally, the percentage variation between specimens increases with the number of days of dry curing. For example, samples subjected to one day of conditioning exhibit a 7.03% reduction in debonding pressure relative to samples not exposed to a dry environment, whereas specimens exposed to two days of dry conditions show a 17.88% reduction in debonding pressure. Similar behavior is observed in the wetting pressure for samples exposed for 1 and 2 days under dry conditions, with reductions of 1.51% and 4.84%, respectively, relative to the control samples.

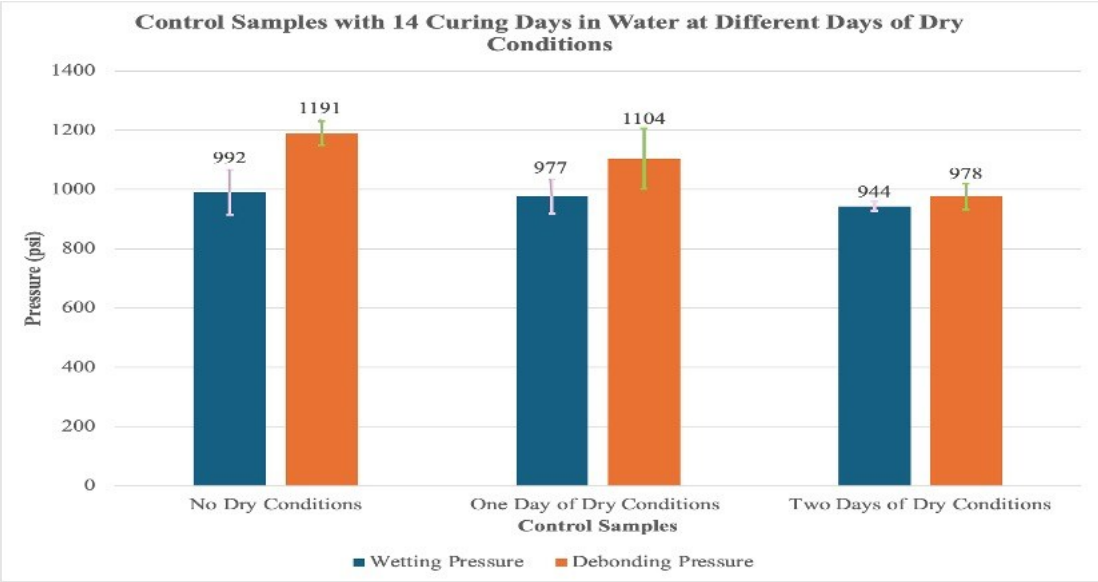

Figure 8: Wetting and debonding pressures for controlling samples on different days of dry conditioning.

3.2 Samples at Five Thermo-cycles

Figure 9 presents the results for the specimens subjected to five thermal cycles. For this scenario, three specimens were tested. In the first group of bars, the average response of the control samples cured for 14 days in a water bath, followed by one day of dry curing, is shown. This block exhibits the highest values for both debonding pressure and wetting pressure, with average values of 1104 psi and 977 psi, respectively.

In contrast, the three specimens subjected to five thermal cycles exhibit similar responses, with a maximum variation of approximately 2% among them. Compared with the control samples, the specimen with the lowest debonding pressure shows an overall reduction of nearly 8%.

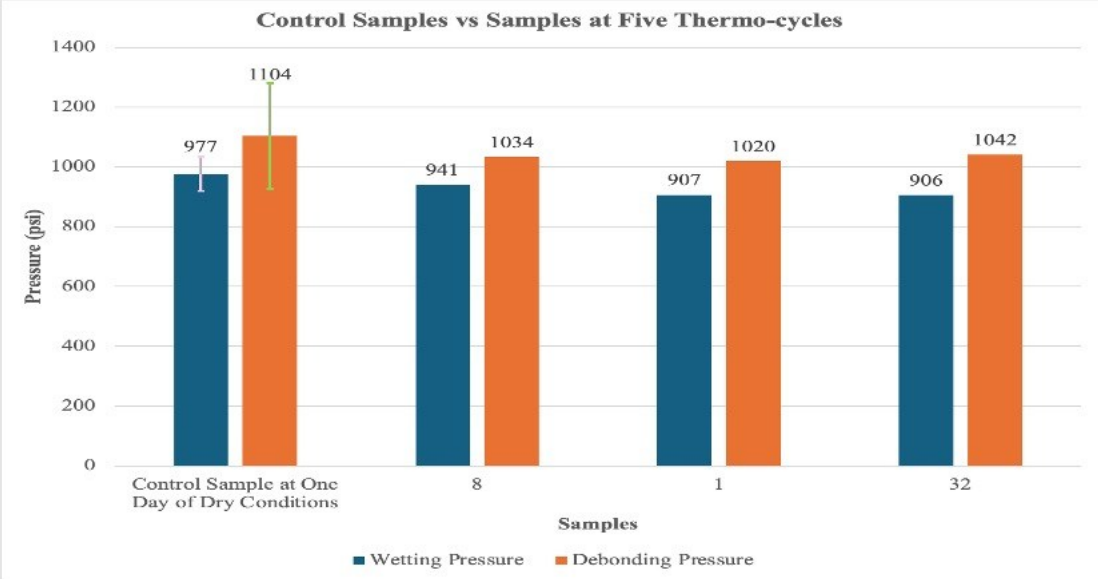

Figure 9: Wetting and debonding pressure for the control sample and samples at five thermo-cycles.

The scenario changes when comparing the average response of control specimens not exposed to dry curing conditions with specimens subjected to five thermal cycles, as shown in Figure 10. The average debonding pressure for the control specimens is 1191 psi. When the debonding pressure of the control specimen was compared with the average debonding pressure of the 5-cycle samples, a 13.35% reduction was observed. On the other hand, the behavior of the wetting pressure, considering only the three specimens subjected to the conditions analyzed in this scenario, shows a maximum variation of 4% among them. However, nearly twice this variation is observed when the average wetting pressure of these specimens is compared with that of the control sample, with a difference of 7.27%.

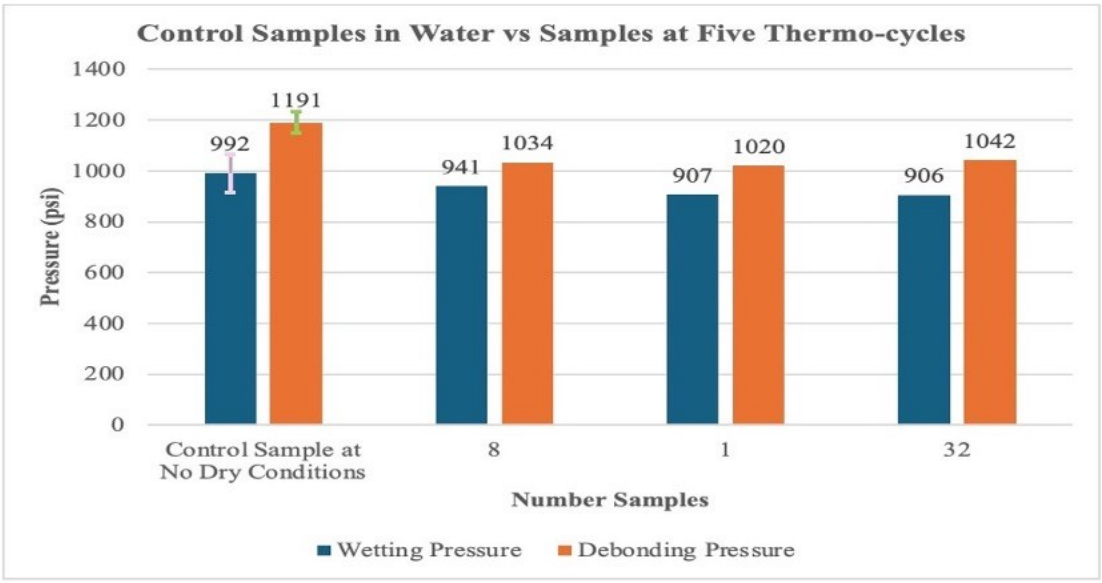

Figure 10: Wetting and debonding pressure for Five thermo-cycle samples and control samples at no dry conditions.

3.3 Samples at Ten Thermo-cycles

A similar analysis can be performed by comparing the control specimen subjected to two days of dry curing, corresponding to the ten thermal cycles. Once again, it is observed that both wetting and debonding occur at higher pressures in the control specimen than in the specimens subjected to thermal cycling. A reduction of 19.33% and 24% in the debonding and wetting pressure, respectively, is observed between the control specimen and the sample with the lowest debonding and wetting pressure values.

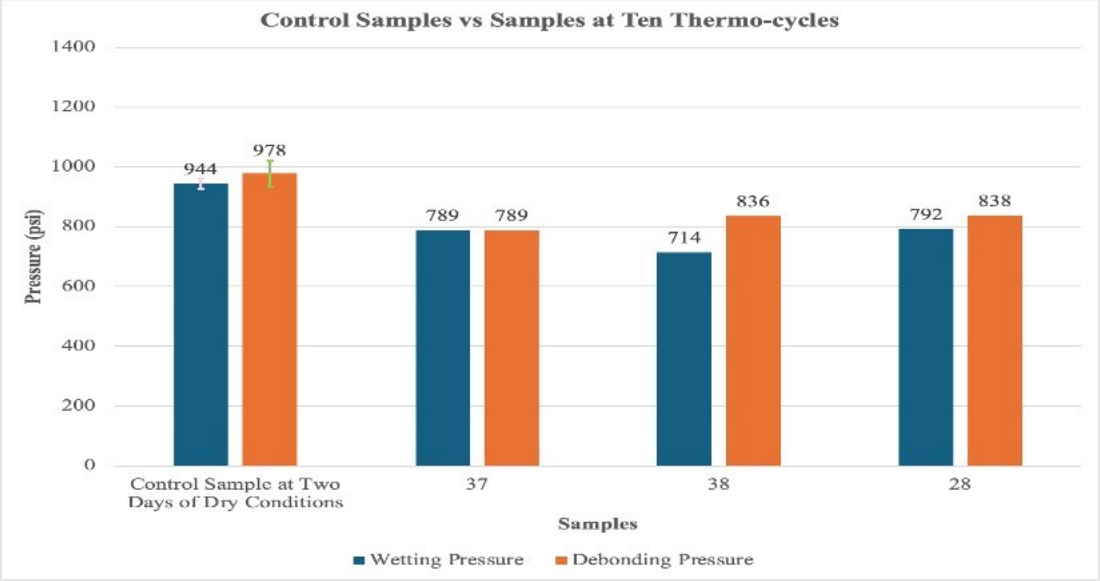

Figure 11: Wetting and debonding pressure for the control sample and samples at ten thermo-cycles.

As done for the specimens exposed to five thermal cycles, Figure 12 compares specimens subjected to 10 thermal cycles with the average response of samples fully cured in water and not exposed to dry-curing conditions. The figure shows that the debonding pressure drops sharply from 1191 psi to 789 psi in the sample with lower debonding pression (#37). This corresponds to a 34% reduction of pressure. On the other hand, the wetting pressure in specimen 38 is 28% lower when compared with the average value of the control specimens cured in water.

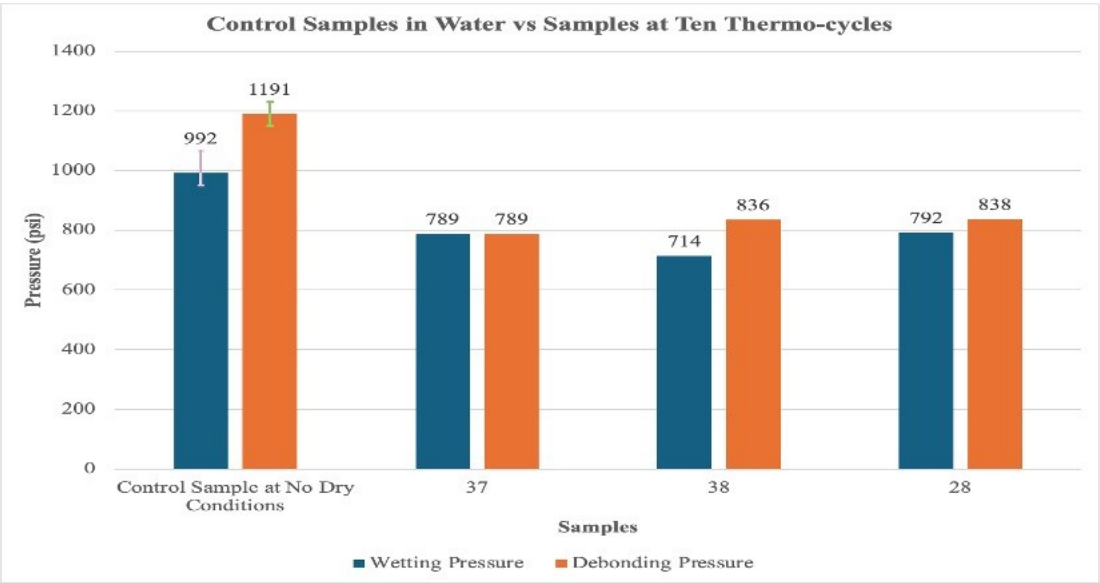

Figure 12: Wetting and debonding pressure for ten thermo-cycle samples and control samples at no dry conditions.

3.4 Combined results

Figure 13 presents the average values for the different control samples and the specimens subjected to thermal cycling. The three groups of results show low data variability. However, the control specimens exhibit the highest coefficients of variation, with an 11% variation in debonding pressure and a 7% variation in wetting pressure.

Conversely, the specimens subjected to five thermal cycles show the lowest variability for both pressures, with coefficients of variation of 2% for wetting pressure and 1% for debonding pressure. Finally, the cement samples tested under ten thermal cycles exhibit variations of 6% and 3% for wetting and debonding pressures, respectively.

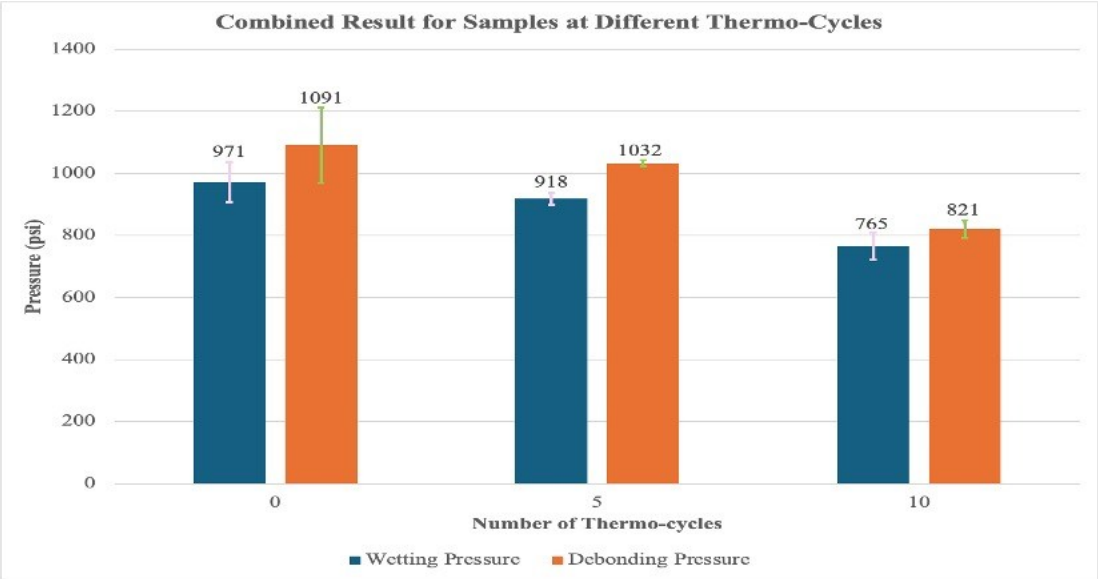

Figure 13: Combined results of samples.

It is interesting to see how the percentage changes in the debonding and wetting pressures while thermo-cycling increases. Table 2 shows these temperature changes affecting the IBSS.

Table 2: Percentage difference in debonding and wetting pressure compared against control samples

Control Samples		Samples at 5 thermo-cycles		Samples at 10 thermo-cycles		% Decrease between control samples vs 5 thermo-cycles		% Decrease between control samples vs 10 thermo-cycles	
Debonding Pressure (psi)	Wetting Pressure (psi)	Debonding Pressure (psi)	Wetting Pressure (psi)	Debonding Pressure (psi)	Wetting Pressure (psi)	Debonding	Wetting	Debonding	Wetting
1091	971	1032	918	821	765	5.41	5.46	20.45	16.67

4. DISCUSSIONS

Based on the results of this experiment, it is evident that continuous thermal cycling affects the interfacial bond strength of Class G cement. In addition, the influence of dry curing conditions, which further intensify these effects, can be clearly identified. This behavior is evident in Figure 8, where the debonding pressure decreases from 1191 psi for specimens not exposed to dry curing conditions to 1104 psi after one day of dry curing and further decreases to 978 psi after two days of dry curing. This trend can be explained according to Sprung, 2000 and Kurdowski, 2014, who attributed such degradation to cement shrinkage caused by insufficient hydration, leading to increased capillary porosity and weakening of the calcium silicate hydrate (C–S–H) microstructure. Cement degradation becomes more pronounced when individuals are subjected to both thermal cycling and dry curing conditions. Figures 10 and 11 show that cement samples exposed to 10 thermal cycles and 2 days of dry curing exhibit a 17.88% reduction in debonding pressure, and an even greater reduction is observed compared with control specimens not subjected to either thermal cycling or dry curing, which show a 34% decrease in debonding pressure. These results confirm that the operating conditions of geothermal wells compromise the integrity of the cement sheath.

Furthermore, it was observed that, consistent with the findings reported by Abid et al., 2025, the debonding pressure is preceded by a wetting phase occurring at a lower pressure, which increases when the cement is subjected to thermal cycling and dry curing conditions. This behavior promotes the formation of microannuli and the loss of interfacial bonding, as previously demonstrated by De Andrade et al., 2015 and Vrålstad et al., 2015. As observed in the results, debonding is accelerated by thermal cycling, leading to cumulative reductions of 7.03% after five cycles and 17.88% after ten cycles compared to the control samples. This trend becomes more pronounced when considering specimens not exposed to dry curing conditions, with reductions of 13.35% after five cycles and 34% after ten cycles. These observations suggest the presence of differential stresses caused by the mismatch in thermal expansion coefficients between the casing and the cement, validating the vulnerability of Class G cement to continuous thermal loading in geothermal environments. This behavior is consistent with the conclusions reported by Albawi et al., 2014, who identified microannulus formation and reduced annular sealing when cement is subjected to similar thermal cycling conditions.

It is notable that data dispersion, evaluated using the coefficient of variation (CV), provides additional insight into the stability of interfacial behavior. For instance, specimens subjected to five thermal cycles exhibit lower dispersion (CV of 1–2%) compared to control samples. This observation may suggest a potential improvement in hydration during the early stages of thermal cycling, leading to partial densification of the C–S–H matrix and consolidation of interconnections before mechanical damage develops. However, this trend deteriorates due to interfacial fatigue when ten thermal cycles are applied. According to Patel et al., 2025, early thermal maturation through the use of additives such as silica fume can improve the initial strength of cement; however, this effect has not been validated for Class G cement under high-pressure, high-temperature (HPHT) conditions.

As discussed previously, this experiment demonstrates how cement bonding strength is affected by thermal cycling at 0, 5, and 10 cycles. Additional tests using intermediate values such as 1, 3, and 7 cycles would help determine the point at which interfacial strength begins to be significantly compromised, enabling the establishment of minimum interfacial bonding strength (IBSS) criteria for the design of geothermal wells.

5. CONCLUSIONS

Through this study, the effect of thermal cycles and curing conditions on the interfacial bonding strength of Class G cement was evaluated by analyzing the wetting pressure and the debonding pressure. It can be concluded that the number of thermal cycles directly affects the bonding between the cement and the casing. As the number of cycles increases, a clear reduction in debonding pressure is observed, confirming the progressive degradation of interfacial bonding within the system. Additionally, a further reduction is noted when specimens are subjected to dry curing conditions, suggesting that moisture loss and cement shrinkage negatively affect the cement microstructure and its ability to remain bonded to the casing.

The debonding pressure is preceded by a wetting phase, which is accelerated when the cement is subjected to thermal cycling and dry curing conditions, promoting the formation of microannuli and the loss of hydraulic sealing at the cement–casing interface. On the other hand, specimens subjected to five thermal cycles exhibited a transient densification effect, resulting in lower dispersion of the measured results. However, when specimens are exposed to a higher number of thermal cycles, a more pronounced degradation of the cement matrix is observed due to repetitive thermal loading, which induces interfacial fatigue between the cement and the casing.

Additional testing is required to determine the number of thermal cycles at which interfacial strength begins to be significantly compromised. This would allow the establishment of minimum interfacial bonding strength (IBSS) criteria to support the design and evaluation of more robust cementing systems for geothermal applications.

REFERENCES

Abid, K., et al. . (2025). Experimental investigation of the interfacial debonding strength of class G cement and the implications to well integrity. . *International Journal of Greenhouse Gas Control 142*

Albawi, A., De Andrade, J., Torsæter, M., Opedal, N., Stroisz, A., & Vrålstad, T. . (2014.). *Experimental set-up for testing cement sheath integrity in arctic wells.* In OTC Arctic Technology Conference

API, A. P. I. (2005). API Specication 10-A. API. In.

Arbad, N., Emadi, H., & Watson, M. . (2022). A comprehensive review of geothermal cementing from well integrity perspective. . *Journal of Petroleum Science and Engineering, , 217*, 110869.

De Andrade, J., Sangesland, S., Todorovic, J., & Vrålstad, T. (2015). *Cement sheath integrity during thermal cycling: a novel approach for experimental tests of cement systems.* In SPE Norway Subsurface Conference

Fischer, H. R., & Moghadam, A. . (2023). Testing Various Cement Formulations under Temperature Cycles and Drying Shrinkage for Low-Temperature Geothermal Wells. . *Materials,, 16*(23), 7281.

Kurdowski, W. (2014). *Cement and concrete chemistry.*

Lambrescu, I., Khizar Abid, and Catalin Teodoriu. . (2024). Cement-Formation Debonding Due to Temperature Variation in Geothermal Wells: An Intensive Numerical Simulation Assessment. *Energies 17.19* (4953.).

Lambrescu, I., Teodoriu, C., & Amani, M. . (2021). Experimental and numerical investigations of cement bonding properties. . *Materials, , 14*(23), 7235.

Patel, Z. M., Mahmoud, A. A., & Wang, Y. ((2025). *Improvement in Geothermal Well Integrity: A Review of New Advanced Cementing Technologies.* SPE Middle East Oil and Gas Show and Conference

Phi, T., Elgaddafi, R., Al Ramadan, M., Ahmed, R., & Teodoriu, C. (2019). *Well integrity issues: Extreme high-pressure high-temperature wells and geothermal wells a review.* In SPE Thermal Integrity and Design Symposium,

Sprung, S. (2000). Cement. . *Ullmann's Encyclopedia of Industrial Chemistry.*

Vrålstad, T., Skorpa, R., Opedal, N., & De Andrade, J. . (2015). *Effect of thermal cycling on cement sheath integrity: Realistic experimental tests and simulation of resulting leakages.* In SPE Thermal Integrity and Design Symposium